Parametric study of the transition in the wake of oblate spheroids and flat cylinders

MARCIN CHRUST†, GILLES BOUCHET AND JAN DUŠEK

Institut de Mécanique des Fluides et des Solides, Université de Strasbourg/CNRS,
Strasbourg 67000, France

An exhaustive parametric study of the transition scenario in the wake of oblate spheroids and flat cylinders placed with their rotation axis parallel to the flow is presented. The flatness of the investigated objects is classified by the aspect ratio χ defined as $\chi = d/a$ for spheroids (with d the diameter and a the length of the polar axis) and as $\chi = d/h$ for cylinders (with h the cylinder height). We find a significant qualitative similarity between both configurations. At large aspect ratios ($\chi > 2.3$ for spheroids and $\chi \geqslant 4$ for cylinders), the secondary bifurcation giving rise to a periodic state without planar symmetry is subcritical with a hysteresis interval of about two Reynolds number units. For spheroids, the sphere-like scenario is recovered only at aspect ratios very close to one ($\chi \geqslant 1$ are considered), while for cylindrical bodies the same holds for $\chi \leqslant 1.7$. For intermediate aspect ratios, a domain of states with non-zero net helicity separates states typical for the sphere wake from those of an infinitely flat disk.

Key words: instability, transition to turbulence, wakes

1. Introduction

The pioneering linear analysis of the breaking of axisymmetry in wakes of axisymmetric bodies of Natarajan & Acrivos (1993) focused on two prototypical bodies: a sphere and a disk. While the wake of a sphere has been the topic of extensive experimental research, the topic of a flat disk and flat cylindrical bodies has been taken up only in a handful of recent, mostly numerical and theoretical papers. For a cylinder, the aspect ratio is defined as $\chi = d/h$, where d is the cylinder diameter and h is the cylinder height. In what follows, a 'flat disk' is considered to correspond to an infinite aspect ratio, while if the body is cylindrical with non-zero height it will be called a flat cylinder if $\chi > 1$. It clearly appears that the transition scenario in these wakes differs considerably from that of the fixed sphere wake; furthermore, the transition process involves several new states that do not exist in the sphere wake. The present literature on the transition from a steady symmetric to a chaotic flow over a flat disk or a thin cylinder reveals seven transition stages.

(*a*) In all investigated configurations, the flat disk ($\chi = \infty$), considered by Natarajan & Acrivos (1993), Fabre, Auguste & Magnaudet (2008) and Meliga, Chomaz & Sipp (2009), and flat cylinders of aspect ratio larger than one, investigated

† Email address for correspondence: Marcin.Chrust@etu.unistra.fr

by Fernandes *et al.* (2007) ($\chi = 2$–10), Shenoy & Kleinstreuer (2008) ($\chi = 10$) and Auguste, Fabre & Magnaudet (2010) ($\chi = 3$), the primary bifurcation is regular in the $m = 1$ azimuthal subspace, leading to a steady non-axisymmetric but planar symmetric state, the symmetry plane of which has an arbitrary orientation selected by initial conditions (see Ghidersa & Dušek 2000). The breaking of axisymmetry yields a steady lift oriented in the symmetry plane. This state is denoted by SS (steady state) in Fabre *et al.* (2008) and Meliga *et al.* (2009) and 'steady asymmetric' in Shenoy & Kleinstreuer (2008). The threshold of the primary bifurcation has been given by Fernandes *et al.* (2007) as a function of χ for cylinders of finite aspect ratio. In the cited literature, there is a good consensus as to the critical Reynolds number value of Re_1 for a flat disk. It is found to be between 115 and 117.

(*b*) While the steady non-axisymmetric state is common to all cases investigated, including that of a sphere, the secondary bifurcation, albeit of Hopf type in all cases, has been found to lead to a specific periodic state without planar symmetry for a flat disk and a cylinder of aspect ratio $\chi = 10$. This state is characterized by a 'kinking of trailing vortices' past the body (see Shenoy & Kleinstreuer 2008) generating an oscillating component of the lift. While the mean lift lies in the symmetry plane selected at the primary bifurcation, the oscillating component is perpendicular. As a consequence, it has been called RSB (reflectional symmetry breaking) by Fabre *et al.* (2008), the MM_π (mixed mode with phase π) state by Meliga *et al.* (2009), 'steady 3D periodic with regular rotation of the separation region' by Shenoy & Kleinstreuer (2008) or 'yin-yang' by Auguste *et al.* (2010). For the flat disk the critical Reynolds number Re_2 was found between 121 and 125.6.

(*c*) Alternatively, for $\chi = 3$, Auguste *et al.* (2010) evidenced a transition to the periodic state with planar symmetry, as observed many times in the sphere wake (see e.g. Johnson & Patel 1999) at the secondary bifurcation. In this state, the lift oscillates in the symmetry plane and keeps a non-zero mean value. It has been called the RSP state by Fabre *et al.* (2008), the MM_0 state by Meliga *et al.* (2009) or 'zig-zig' by Auguste *et al.* (2010). The change of the bifurcated state does not significantly influence the trend of the critical Reynolds number as a function of the aspect ratio. It was fitted to a smooth function by Fernandes *et al.* (2007).

(*d*) State (*c*) is to be distinguished from the periodic state with a zero-mean lift although both have a symmetry plane. The mean value of the oscillating lift in the periodic state without planar symmetry (*b*) has been observed to vanish upon an increase in the Reynolds number until the planar symmetry is recovered (but with a symmetry plane perpendicular to that chosen at the primary bifurcation). The lift oscillates in this symmetry plane with a zero-mean value. This periodic state with a zero-mean lift has been observed for the flat disk and for the cylinder of aspect ratio $\chi = 10$. It is to be noted that the same state arises when the Hopf bifurcation directly breaks the axisymmetry of the flow, which happens for the opposing flow in the wake of a heated sphere (see Kotouč, Bouchet & Dušek 2009*a*). In the literature concerning disks, this state is called the SW (standing wave) mode (Fabre *et al.* 2008; Meliga *et al.* 2009) or 'unsteady with plane of symmetry and zero lift force' (Shenoy & Kleinstreuer 2008). Its threshold has been found at $Re \approx 140$ (Fabre *et al.* 2008) and 143 (Meliga *et al.* 2009).

(*e*) In a single case, for the cylinder with $\chi = 3$ (Auguste *et al.* 2010), the existence of a state with non-zero helicity has been reported. The net non-zero helicity arises due to unequal amplitudes of spiral modes appearing in the weakly nonlinear analysis of Fabre *et al.* (2008) and Meliga *et al.* (2009). On the time scale of a vortex shedding period, the helicity yields an elliptic path of the lift. The latter moves periodically in

the plane perpendicular to the flow axis so that the lift path can roughly be described as a slowly oscillating or rotating ellipse. Because of the two scales present and the form of the lift trajectory, the state is called 'quasi-periodic pulsating' or 'knit-knot' by Auguste *et al.* (2010). Similar states have also been observed in the opposing flow past a heated sphere by Kotouč *et al.* (2009*a*).

(*f*) The transition to chaos is preceded by a quasi-periodicity characterized by the presence of a slower frequency close to 1/3 of the 'leading frequency' of the previous regimes (Fabre *et al.* 2008). The same behaviour has been observed in the unheated and heated sphere wake (Bouchet, Mebarek & Dušek 2006; Kotouč, Bouchet & Dušek 2009*b*). A similar modulation occurs in states with non-zero net helicity (Kotouč *et al.* 2009*b*).

(*g*) The chaotic states have no symmetry. The lift coefficient describes a chaotic path in the plane perpendicular to the flow axis.

In spite of significant progress in the understanding of the transition scenario of flat axisymmetric bodies, especially of a flat disk, the existing literature does not provide a more systematic picture, taking into account variations in the aspect ratio. For flat cylinders, the parametric study of the first two bifurcation thresholds of Fernandes *et al.* (2007) can be improved, extended and refined with reference to the progress in identification of more complex regimes. The linear analysis of Natarajan & Acrivos (1993) takes up the flat disk and a sphere as two extreme cases. The link between them is represented by oblate spheroids rather than by flat cylinders. The former have, however, never been investigated. The wakes of cylinders and spheroids can both be characterized by just two parameters, allowing a relatively easily feasible two-parametric study providing an exhaustive picture of the transition scenario. The purpose of this paper is to present the results of such an investigation.

2. Mathematical formulation and numerical method

The mathematical formulation and numerical method used are basically those of Ghidersa & Dušek (2000). The three-dimensional Navier–Stokes equations are non-dimensionalized with respect to the inflow velocity U and the diameter of the transverse cross-section d:

$$\nabla \cdot \boldsymbol{v} = 0, \tag{2.1}$$

$$\frac{\partial \boldsymbol{v}}{\partial t} + (\boldsymbol{v} \cdot \nabla) \cdot \boldsymbol{v} = -\nabla p + \frac{1}{Re} \nabla^2 \boldsymbol{v}, \tag{2.2}$$

and are solved in a cylindrical coordinate system (z, r, θ), with the z-axis parallel to the free-stream direction, r the distance to the axis and θ the azimuthal angle. The non-dimensionalization yields the Reynolds number defined as $Re = Ud/\nu$ and the aspect ratio defined in the Introduction (§ 1) for cylinders and given by $\chi = d/a$ for the spheroids, where d is the transverse diameter and a is the length of the streamwise axis of the spheroid.

The equations are discretized using the spectral–spectral-element discretization (see Ghidersa & Dušek 2000; Jenny & Dušek 2004, for more details), combining the Fourier expansion in the azimuthal direction with a spectral-element discretization in the (z, r)-plane. The cylindrical computational domain of radius $R = 8d$ extends $12d$ upstream and $25d$ downstream of the considered objects. The extent of the domain has many times been tested in previous work. It needs to be modified depending on flow conditions, namely, on the considered Reynolds numbers. For example, for low Reynolds numbers, very large domains must be used (see e.g. Kotouč *et al.* 2009*a*). At

Re	$N = 6$		$N = 8$	
Re_1	117.17		116.92	
Re_2	125.18 (4)	125.15 (6)	125.12 (4)	125.11 (6)

TABLE 1. Mesh test results for a flat disk. The values in parentheses indicate the number of azimuthal modes of a Fourier expansion. N denotes the number of collocation points in spectral elements.
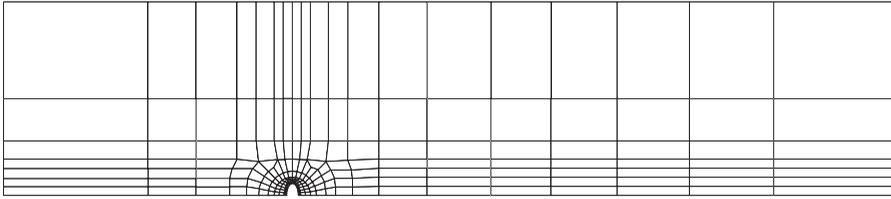

FIGURE 1. Spectral element discretization of the radial–axial plane of the computational domain of an oblate spheroid of $\chi = 2$. The inflow is situated on the left.

Reynolds numbers exceeding 100, the dimensions of the mentioned domain together with no-stress boundary conditions at the outflow and lateral boundary were always found to provide the instability thresholds with an error smaller than 1 %. The $(z–r)$-plane is broken up into spectral elements with N Gauss–Lobatto–Legendre collocation points in each direction (z, r) (see figure 1). The azimuthal direction is discretized by Fourier expansion. The flow is forced by a uniform Dirichlet boundary condition at the inflow basis of the cylindrical domain.

The spectral-element breakup of the $(z–r)$-plane had to be adapted to the new configuration. Especially for that of the flat disk and the cylindrical bodies, the flow conditions at the body surface differ from those of a sphere. The mesh had to be refined close to the sharp edges to capture the sharp gradients accurately. Nevertheless, the mesh modification, as compared to the mesh presented in Ghidersa & Dušek (2000), is limited roughly to a domain of radius 1d. Several meshes have been developed for each configuration considered and tested for the dependence of the primary and secondary thresholds on the number of collocation points. (A bad mesh yields a solution sensitive to the refinement within spectral elements.) The retained meshes contain 215–241 elements. The influence of the number of azimuthal modes m on the secondary instability threshold was also investigated. The results for the flat disk are presented in table 1. They show that six collocation points and an azimuthal expansion truncated at $m = 4$ provide values that are almost insensitive to further mesh refinement and agree with those of data from the literature.

3. Results

3.1. *Transition states*

In the Introduction we listed seven states $(a–g)$, which have been described in the literature as representing the stages of transition in the wakes of flat disks. The transition stages we observed in the wake of oblate spheroids are very similar. The parametric investigation presented below (see the two following subsections) shows that the classification in §1 is valid for the whole parameter domain investigated for oblate spheroids, namely $\chi \geqslant 1$. Figure 2 provides sample illustrations of analogues of the states reported in the literature on cylindrical bodies in the case of oblate
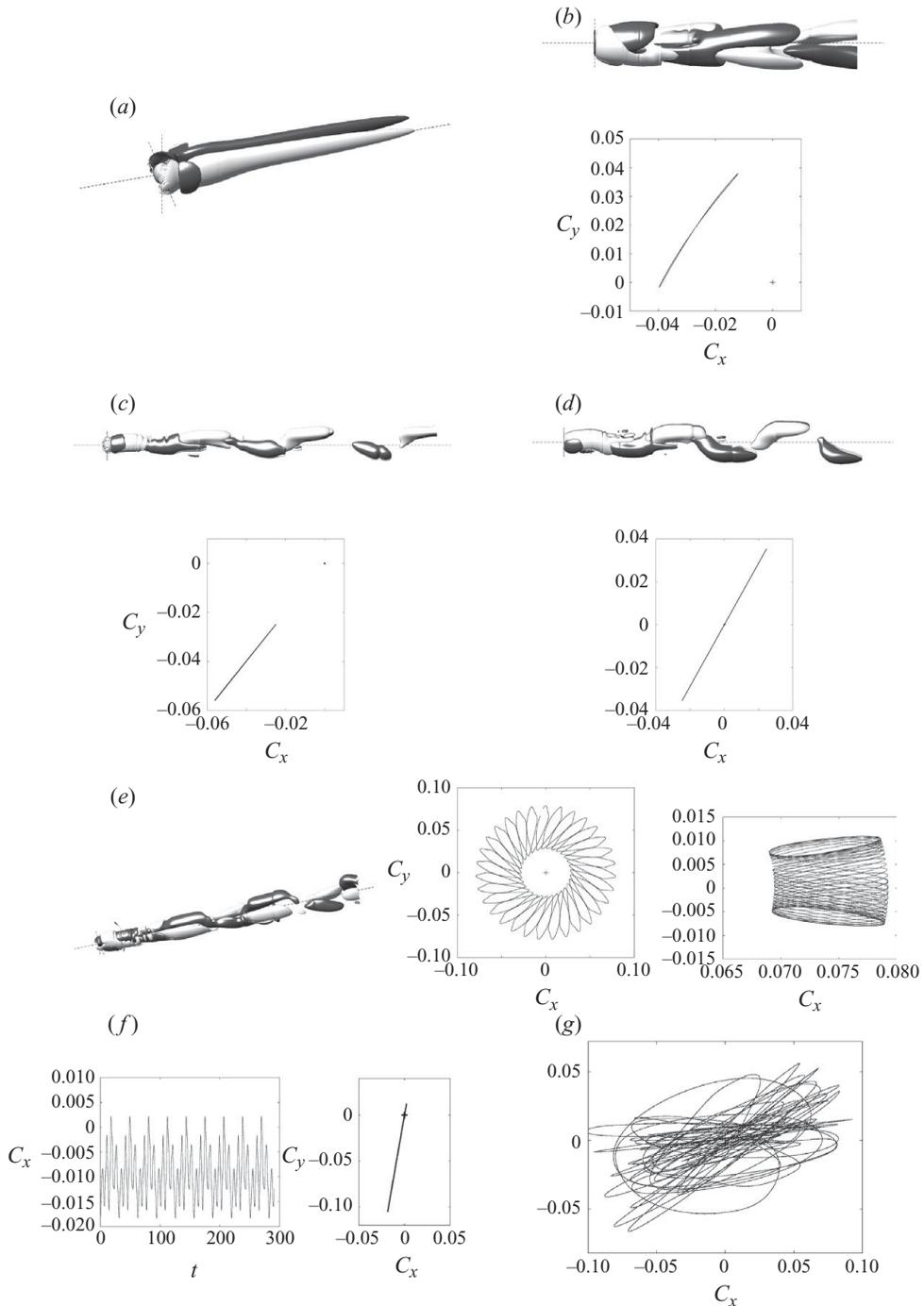
FIGURE 2. Sample characterization of transition states in the wake of oblate spheroids. The letters (*a–g*) refer to the states presented in §1. (*a*) Steady asymmetric, $\chi = 1.25$, $Re = 225$; (*b*) periodic without planar symmetry, $\chi = 6$, $Re = 145$; (*c*) periodic with planar symmetry and non-zero mean lift, $\chi = 1.25$, $Re = 268$; (*d*) periodic with zero-mean lift, $\chi = 6$, $Re = 183$; (*e*) non-zero helicity, left two figures $\chi = 1.25$, $Re = 283$, right figure $\chi = 1.85$, $Re = 190$; (*f*) quasi-periodic pre-chaotic, $\chi = 1.11$, $Re = 324$; (*g*) chaotic state, $\chi = 1.5$, $Re = 310$. The 3D plots represent a pair of iso-vorticity surfaces corresponding to a positive and negative streamwise vorticity value.

spheroids. Converged states obtained after the decay of transients are represented. The time evolution (including the transients) was monitored by plotting the three components of the hydrodynamic force and the flow field at several points of the wake. The lift coefficient is represented in the figures as best illustrating the nature of the states. The simplest states have already been amply described elsewhere. Here we briefly comment only on the states with non-zero helicity (*e*) and the quasi-periodic pre-chaotic states (*g*).

As stated earlier, the state with non-zero helicity was reported only once, as the 'knit-knot' mode at $\chi = 3$ and $Re = 187$ in the wake of a cylinder (Auguste *et al.* 2010). Many cases of similar states have, however, been evidenced in the opposing flow past a heated sphere at moderate Richardson numbers by Kotouč *et al.* (2009*b*). As a rule, the domain of stability of purely biperiodic states is very limited (the main period being the 'leading frequency' of vortex shedding linked to the Hopf bifurcation and the secondary period being the frequency, sometimes very slow, characteristic for the 'migration' of the ellipse representing the projection of the lift onto the plane perpendicular to the flow axis at the scale of one vortex shedding period). Very often, at least in the opposing flow past a sphere, the ellipse is very flat, which means that there still remains a slightly distorted symmetry plane of the wake. The latter either slowly oscillates or rotates (see figure 19 of Kotouč *et al.* 2009*b*). In the case of oblate spheroids, we observed both a rotating (see figure 2*e* for $\chi = 1.25$, $Re = 283$) and oscillating version (see the same figure but the case of $\chi = 1.85$, $Re = 190$) of the state with non-zero net helicity. In the 'rotating' case, the path of the lift describes an ellipse slowly rotating with constant angular velocity in the given direction, and in the 'oscillating' case, its rotation stops and reverses back so that the ellipse axis oscillates only within a limited angle. The main difference between figure 19 of Kotouč *et al.* (2009*b*) and the present figure 2(*e*) consists of the non-zero mean lift of the average is taken over one short vortex shedding period. Such a state was also observed in opposing flow but only in its rotating version.

The onset of chaos is not always quite clear-cut. If states with well-defined symmetry, (*c* and *d*), become chaotic, the onset of chaos can be associated with the loss of this symmetry. The chaotic state described by Shenoy & Kleinstreuer (2008) arises from state (*d*) and that by Auguste *et al.* (2010) from state (*c*). Auguste *et al.* (2010) clearly show that a quasi- (multi-) periodicity (with a possible subharmonic lock-in) precedes the onset of chaos. The same observation has been made for a sphere (Bouchet *et al.* 2006). The exact limit between a multi-periodic and a chaotic state is difficult to set. This is even more true in the cases where chaos sets in from a state (*e*), in which no symmetry is present. Nevertheless, we again observe a characteristic subharmonic that distorts the travelling 'ellipse' of the lift path. The latter becomes more and more complicated as large time scale modulations set in until both the time plots and the lift path become completely disorganized. To sum up, unlike other thresholds that can be determined potentially with arbitrary precision, the line delimiting the onset of chaos in the state diagrams presented below is to be understood as approximate.

3.2. *Oblate spheroids*

The transition scenario for oblate spheroids (see figure 4) can be roughly divided into a sphere-like and a flat-disk-like scenario. The difference starts to appear at the secondary bifurcation, the primary steady non-axisymmetric state (*a*) being present in the qualitatively same form for all aspect ratios. The sphere-like and flat-disk-like scenarios are separated by the subdomain of states (*e*) with non-zero helicity extending from the secondary bifurcation threshold at $\chi \approx 2$ almost to the sphere
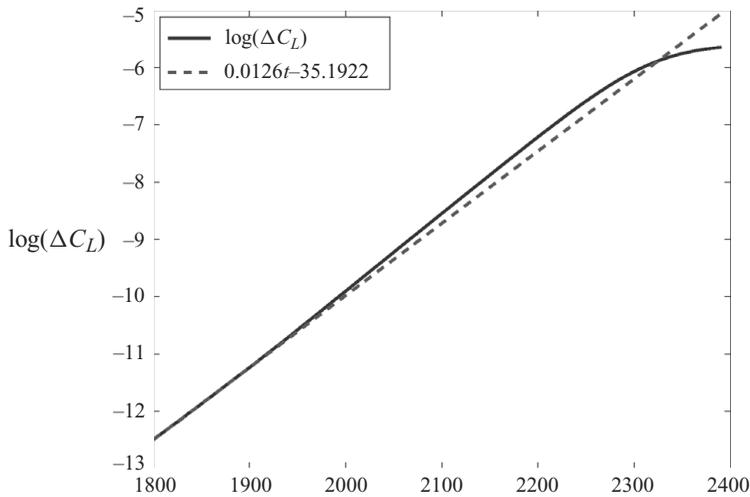
FIGURE 3. Logarithmic plot of the amplitude of the oscillation of the lift coefficient of a flat disk ($\chi = \infty$) at $Re = 126$ (solid line) compared with the purely exponential growth (dashed line, obtained by a linear fit of the initial stage of growth). Note the super-exponential growth in the time interval $t \in [1950, 2350]$ time units.

case $\chi = 1$. We have taken special care to see why the states of non-zero helicity have never been observed in the sphere wake. It appears that the corresponding (*e*)-sub-domain is cutoff between $1/\chi = 0.9$ and 0.95. The most striking feature of the flat-disk-like scenario is that the secondary bifurcation leading to the periodic state without planar symmetry (*b*) appears to be subcritical. Any subcritical bifurcation has two characteristic features (Strogatz 1994, §8.2): a bistability interval below the linear instability threshold and a super-exponential growth above the threshold. An example of the super-exponential growth is presented in figure 3. The bistability band is represented by the grey area in figure 4. The subcriticality seems to be closely linked to the Hopf bifurcation to the (*b*)-state. It is, however, difficult to trace it to the point at which the bifurcations to the non-symmetric state and the symmetric state meet (slightly above $\chi = 2$ for spheroids and close to $\chi = 4$ for cylinders) because the bistability interval becomes very narrow. At $\chi = 2.25$, it either no longer exists or is even narrower than one Reynolds number unit. The bistability interval is represented graphically for several aspect ratios of spheroids and a cylinder of $\chi = 6$ in figure 5. Figure 5(*a*) presents the amplitudes of oscillations of the lift coefficient. A non-zero amplitude is synonymous with the state (*b*). The interval of stability of the steady state (*a*) is shown by dashed lines traced along the horizontal axis (zero amplitude). The same bistability can also be clearly seen in the plot of the mean lift as a function of the Reynolds number. The curves of the steady lift in the state (*a*) do not connect continuously with those of the mean lift in the unsteady periodic state (*b*) and the intervals of existence of both states overlap (see figure 5*b*). The limits of the bistability interval are provided in table 2.

3.3. Flat cylinders

The state diagram for flat cylinders of the aspect ratio $\chi \geqslant 1$ is represented in figure 6. It is seen that the intermediate scenario involving states with non-zero helicity does not extend beyond $\chi = 1.8$ and that the flat-disk-like scenario is limited by an aspect ratio slightly smaller than 4. The first two thresholds, fitted by Fernandes *et al.* (2007)
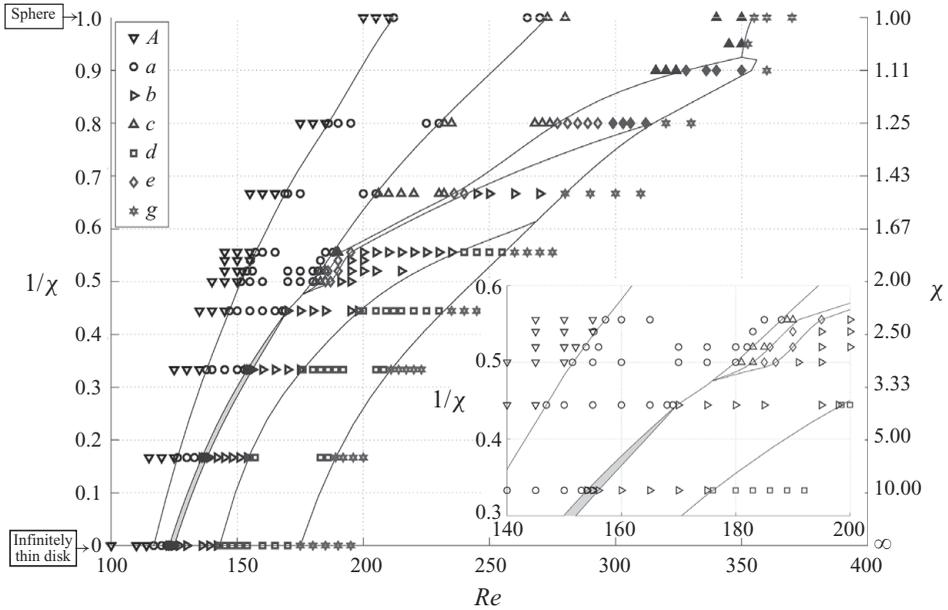
FIGURE 4. State diagram for oblate spheroids. A denotes axisymmetric state. The letters $(a–g)$ in the inset refer to the same states as in the caption of figure 2. The filled triangles (c) and diamonds (e) represent pre-chaotic states (f) with a subharmonic modulation. They can be either with non-zero helicity (diamonds) or with planar symmetry (triangles). The narrow filled band represents the domain of bistability at the subcritical bifurcation.
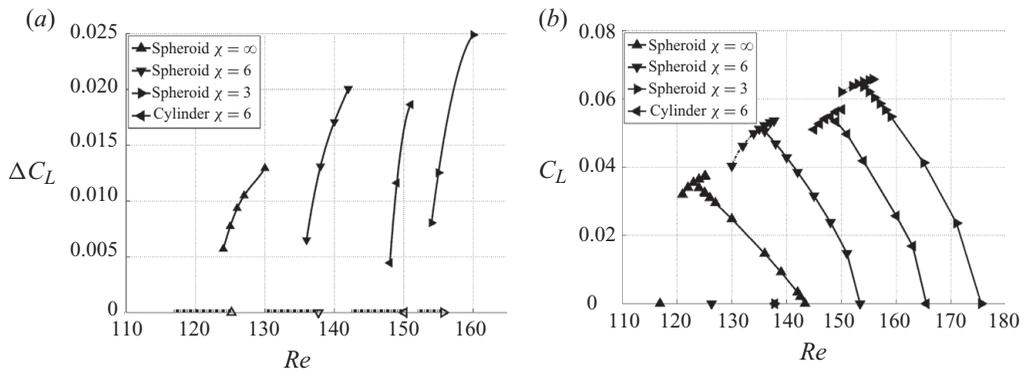

FIGURE 5. (a) Oscillation amplitude ΔC_L of the lift coefficient as a function of the Reynolds number for oblate spheroids of $\chi = \infty$, 6, 3 and a flat cylinder of $\chi = 6$ (see inset). The stability interval of the steady non-axisymmetric state is presented by dashed lines along the horizontal axis. Their linear instability thresholds are plotted as empty triangles. (b) Mean lift as a function of Reynolds number. Four triangles on the horizontal axis to the left of the value 140 represent the primary instability thresholds.

to straight lines in terms of $1/\chi$, are in agreement with our data close to $\chi = \infty$ but deviate from the thresholds evidenced in figure 6 at $\chi = 2$. However, a closer look at figure 18 of Fernandes *et al.* (2007) shows that the real computed values at $\chi = 2$ lie clearly above the fit. There is a very good agreement in the thresholds of all states described by Fabre *et al.* (2008) and Meliga *et al.* (2009). The thresholds of Shenoy & Kleinstreuer (2008) are systematically above those of figure 6. The difference grows

Spheroids			Cylinders		
χ	Re_2'	Re_2	χ	Re_2'	Re_2
∞	[124]	125.2	∞	[124]	125.2
6	[136]	137.7	6	[148]	150.1
3	[154]	155.7	4	[164]	165.6

TABLE 2. Linear stability thresholds Re_2 and lower bounds of bistability Re_2' ($Re_2' < Re_2$) of the subcritical Hopf bifurcation for oblate spheroids and flat cylinders. (The values in square brackets are closest integer upper bounds.)
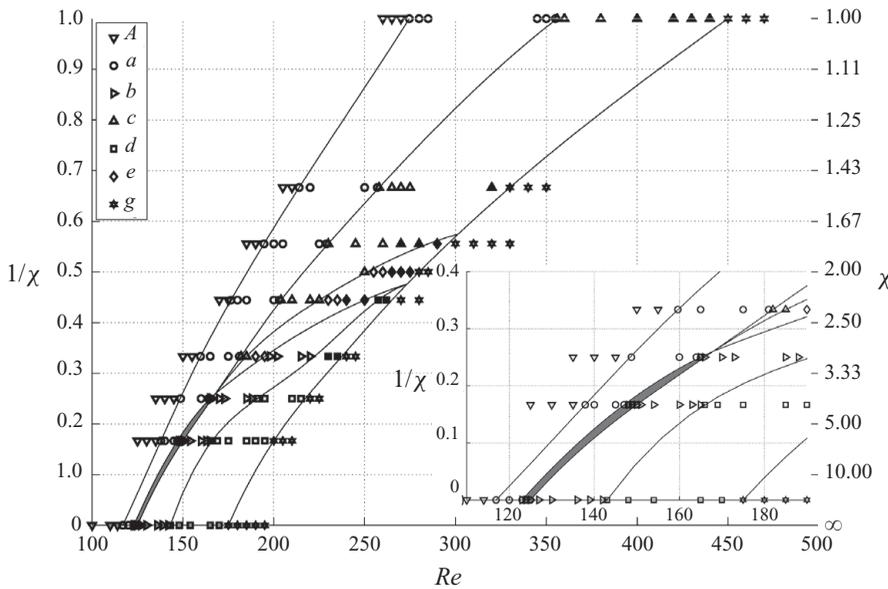

FIGURE 6. State diagram for cylinders. The meaning of the symbols is the same as in figure 4. The band of bistability at the subcritical bifurcation is still present for $1/\chi \leqslant 0.25$.

considerably with the Reynolds number. The comparison of our data with those of the literature is provided in table 3.

4. Conclusion

The state diagrams presented are intended to serve as a tool that allows us to assess the expected asymptotic state for any numerical or experimental configuration involving oblate spheroids and flat cylinders. Beyond this practical aspect, they may provide a basis for theoretical reflection that has already been remarkably developed for flat disks by Fabre *et al.* (2008) and Meliga *et al.* (2009). The subcriticality of the secondary Hopf bifurcation can to some extent be neglected but, if it is to be taken into account, the weakly nonlinear models must be developed to a higher order. Finally, detailed knowledge of the transition scenario of fixed objects provides an indispensable reference for simulations of freely falling disks. This topic has gained significant attention from the scientific community since the experimental paper by Field, Klaus & Moore (1997). It is the principal goal of the experimental paper by Fernandes *et al.* (2007) but remains a stimulating numerical challenge.

χ	Re_1	Re_2/St_2	Re_3/St_3	Re_4/St_4	Re_5/St_5	Re_6
∞ [1]	≈ 115	≈ 121 *0.119*	≈ 140			
∞ [2]	116.9	125.3 *0.121*	143.7* *0.118*			
∞ [3]	116.92	(124, 125.2) *0.120*	[142, 143] *0.118*	[165, 170]		
10 [4]	135	155 *0.113*	172	280		
10 [3]	129.6	(136.3, 138.7) *0.115*	154.4 *0.114*	188.8		
3 [5]	≈ 159.4	≈ 179.8 *0.109*	[184, 185]	[190, 191]	≈ 215	≈ 240
3 [3]	159.65	[181, 182] *0.112*	[185, 190] *0.112*	[195, 198] *0.112*	[220, 230] *0.111*	[235, 240]

TABLE 3. Bifurcation thresholds. Numbers in brackets indicate authors: [1] Fabre *et al.* (2008), [2] Meliga *et al.* (2009), [3] present study, [4] Shenoy & Kleinstreuer (2008), [5] Auguste *et al.* (2010). *Result obtained using asymptotic expansion. At $\chi = 10$, the values of the present study are obtained by interpolation between $\chi = \infty$ and $\chi = 6$. Re_2 is understood as the critical Reynolds number for the loss of stability of the steady non-axisymmetric state. Values in italics below the critical Reynolds numbers are Strouhal numbers of the oscillations at the corresponding threshold. For the quasi-periodic state at $\chi = 3$, $Re = Re_4$, the dominant frequency is indicated. The parentheses denote the bistability interval; the square brackets delimit the error margin.

REFERENCES

AUGUSTE, F., FABRE, D. & MAGNAUDET, J. 2010 Bifurcations in the wake of a thick circular disk. *Theor. Comput. Fluid Dyn.* **24**, 305–313.

BOUCHET, G., MEBAREK, M. & DUŠEK, J. 2006 Hydrodynamic forces acting on a rigid fixed sphere in early transitional regimes. *Eur. J. Mech.* B *Fluids* **25**, 321–336.

FABRE, D., AUGUSTE, F. & MAGNAUDET, J. 2008 Bifurcations and symmetry breaking in the wake of axisymmetric bodies. *Phys. Fluids* **20**, 051702.

FERNANDES, P. C., RISSO, F., ERN, P. & MAGNAUDET, J. 2007 Oscillatory motion and wake instability of freely rising axisymmetric bodies. *J. Fluid Mech.* **573**, 479–502.

FIELD, S. B., KLAUS, M. & MOORE, M. G. 1997 Chaotic dynamics of falling disks. *Nature* **388**, 252–254.

GHIDERSA, B. & DUŠEK, J. 2000 Breaking of axisymmetry and onset of unsteadiness in the wake of a sphere. *J. Fluid Mech.* **423**, 33–69.

JENNY, M. & DUŠEK, J. 2004 Efficient numerical method for the direct numerical simulation of the flow past a single light moving spherical body in transitional regimes. *J. Comput. Phys.* **194**, 215–232.

JOHNSON, T. A. & PATEL, V. C. 1999 Flow past a sphere up to a Reynolds number of 300. *J. Fluid Mech.* **378**, 19–70.

KOTOUČ, M., BOUCHET, G. & DUŠEK, J. 2009*a* Drag and flow reversal in mixed convection past a heated sphere. *Phys. Fluids* **21**, 054104.

KOTOUČ, M., BOUCHET, G. & DUŠEK, J. 2009*b* Transition to turbulence in the wake of a fixed sphere in mixed convection. *J. Fluid Mech.* **625**, 205–248.

MELIGA, P., CHOMAZ, J. M. & SIPP, D. 2009 Global mode interaction and pattern selection in the wake of a disk: a weakly nonlinear expansion. *J. Fluid Mech.* **633**, 159–189.

NATARAJAN, R. & ACRIVOS, A. 1993 The instability of the steady flow past spheres and disks. *J. Fluid Mech.* **254**, 323–344.

SHENOY, A. R. & KLEINSTREUER, C. 2008 Flow over a thin circular disk at low to moderate Reynolds number. *J. Fluid Mech.* **605**, 253–262.

STROGATZ, S. H. 1994 *Nonlinear Dynamics and Chaos*. Addison-Wesley.